The HIV-1 protein Vpr impairs phagosome maturation by controlling microtubule-dependent trafficking

Audrey Dumas,[1,2,3] Gabrielle Lê-Bury,[1,2,3] Florence Marie-Anaïs,[1,2,3] Floriane Herit,[1,2,3] Julie Mazzolini,[1,2,3] Thomas Guilbert,[1,2,3] Pierre Bourdoncle,[1,2,3] David G. Russell,[4] Serge Benichou,[1,2,3] Ahmed Zahraoui,[1,2,3] and Florence Niedergang[1,2,3]

[1]Institut National de la Santé et de la Recherche Médicale U1016, Institut Cochin, Paris, France
[2]Centre National de la Recherche Scientifique UMR 8104, Paris, France
[3]Université Paris Descartes, Sorbonne Paris Cité, 75006 Paris, France
[4]Department of Microbiology and Immunology, College of Veterinary Medicine, Cornell University, Ithaca, NY 14853

Human immunodeficiency virus type 1 (HIV-1) impairs major functions of macrophages but the molecular basis for this defect remains poorly characterized. Here, we show that macrophages infected with HIV-1 were unable to respond efficiently to phagocytic triggers and to clear bacteria. The maturation of phagosomes, defined by the presence of late endocytic markers, hydrolases, and reactive oxygen species, was perturbed in HIV-1–infected macrophages. We showed that maturation arrest occurred at the level of the EHD3/MICAL-L1 endosomal sorting machinery. Unexpectedly, we found that the regulatory viral protein (Vpr) was crucial to perturb phagosome maturation. Our data reveal that Vpr interacted with EB1, p150^{Glued}, and dynein heavy chain and was sufficient to critically alter the microtubule plus end localization of EB1 and p150^{Glued}, hence altering the centripetal movement of phagosomes and their maturation. Thus, we identify Vpr as a modulator of the microtubule-dependent endocytic trafficking in HIV-1–infected macrophages, leading to strong alterations in phagolysosome biogenesis.

Introduction

Macrophages play crucial functions at the interface between innate and adaptive immunity and also represent niches for intracellular pathogens. They are professional phagocytes that take up pathogens and debris through various opsonic and nonopsonic receptors (e.g., Fc receptors [FcRs] for the Fc portion of immunoglobulins; Flannagan et al., 2012; Canton et al., 2013). Interactions between these receptors and their ligands induce signaling cascades, leading to strong and transient actin polymerization, plasma membrane remodeling, and pseudopod extension around the particulate material (Flannagan et al., 2012; Deschamps et al., 2013; Niedergang, 2016). The closed compartment that forms (the phagosome) loses its actin coat, undergoes fusion and fission with compartments of the endocytic machinery (Botelho and Grinstein, 2011; Fairn and Grinstein, 2012), and eventually fuses with lysosomes. This progressive maturation into a phagolysosomal compartment is accompanied by an acidification of the compartment and its enrichment in hydrolases and reactive oxygen species, forming a degradative compartment. The molecular machineries required for fusion and fission are thought to be the same as for endosome maturation (Fairn and Grinstein, 2012; Scott et al., 2014). Concomitantly, there is a motor-based migration on microtubules toward the cell center to reach a perinuclear localization where lysosomes are located (Blocker et al., 1998; Harrison et al., 2003).

Human immunodeficiency virus type 1 (HIV-1) infects and kills T cells, which profoundly damages the host-specific immune response but also integrates into memory T cells and long-lived macrophages, establishing a chronic infection (Carter and Ehrlich, 2008; Koppensteiner et al., 2012b). Because macrophages are thought to retain viruses in an infectious form, and to potentially release them in a delayed manner and in different locations, they are proposed to be important for virus dissemination and pathogenesis. HIV-1 infection impairs the functions of macrophages both in vivo and in vitro (Kedzierska and Crowe, 2002; Collman et al., 2003), which may contribute to the development of opportunistic diseases. Impaired phagocytosis was also reported in a population of small alveolar macrophages in HIV-infected patients (Jambo et al., 2014). We previously showed that HIV-1, via the viral negative factor (Nef), a major virulence factor that is highly expressed early during virus replication

Correspondence to Florence Niedergang: florence.niedergang@inserm.fr

J. Mazzolini's present address is Centre for Neuroregeneration, University of Edinburgh, Edinburgh EH16 4SB, Scotland, UK.

Abbreviations used in this paper: DHC, dynein heavy chain; ERK1/2, extracellular signal regulated-kinase 1/2; FcR, Fc receptor; H_2DCFDA, dichlorodihydrofluorescein diacetate; HIV-1, human immunodeficiency virus type 1; LB, Luria-Bertani; MDM, monocyte-derived macrophage; Nef, negative factor; RBC, red blood cell; SAPK, stress-activated protein kinase; SRBC, sheep red blood cell; +TIP, plus-end tracking protein; Vpr, regulatory viral protein; WT, wild type.

© 2015 Dumas et al. This article is distributed under the terms of an Attribution–Noncommercial–Share Alike–No Mirror Sites license for the first six months after the publication date (see http://www.rupress.org/terms). After six months it is available under a Creative Commons License (Attribution–Noncommercial–Share Alike 3.0 Unported license, as described at http://creativecommons.org/licenses/by-nc-sa/3.0/).

The Rockefeller University Press $30.00
J. Cell Biol. Vol. 211 No. 2 359–372
www.jcb.org/cgi/doi/10.1083/jcb.201503124

(Witkowski and Verhasselt, 2013), indeed affects phagocytosis by inhibiting the membrane remodeling events that are required for efficient phagosome formation (Mazzolini et al., 2010). Another regulatory viral protein (Vpr) is specifically incorporated into virus particles. Vpr has several described activities, including cell cycle arrest, control of the reverse transcription process, and modulation of the HIV-1 mutation rate (Planelles and Benichou, 2009; Kogan and Rappaport, 2011; Guenzel et al., 2014).

Here, we show that the late steps of phagocytosis are impaired in HIV-infected primary human macrophages, leading to an alteration in cell activation, cytokine production, and bacterial clearance. Phagosome maturation was inhibited, as the endocytic sorting elements based on EHD3/MICAL-L1 were hijacked by the viral activity. Using mutant strains of HIV-1, we demonstrate that Vpr is unexpectedly involved in the perturbation of phagosome maturation. We further show that Vpr interacts with EB1, $p150^{Glued}$, and the dynein heavy chain (DHC). During HIV infection, Vpr is crucial to perturb the localization at the plus ends of microtubules of EB1 and $p150^{Glued}$. This affects the centripetal movement of phagosomes on microtubules, and thus an efficient maturation. We identify Vpr as a major regulator of microtubule-dependent trafficking.

Results

Modification of activation and clearance activity in HIV-1–infected macrophages

To gain insight into the defect in phagocytic functions in HIV-infected macrophages, we aimed to dissect the signaling cascades downstream of the engagement of surface receptors. Monocytes from healthy donors were differentiated into macrophages (monocyte-derived macrophages [MDMs]) with recombinant macrophage-colony stimulating factor for 11 d and were then infected with HIV-1_{ADA} wild type (WT) for 8 d. MDMs were incubated for various times with IgG-opsonized sheep red blood cells (SRBCs) to induce a phagocytic trigger. After various times of contact, cells were lysed and analyzed by Western blotting to detect activation of the MAPKs p38, extracellular signal regulated-kinase 1/2 (ERK1/2), and stress-activated protein kinase (SAPK)/JNK. These kinases play a role in the maturation process of the phagosomes (Moretti and Blander, 2014) and also in activation of transcription factors, such as nuclear factor-κB, which leads to subsequent induction of secretion of proinflammatory cytokines. We noticed that the basal phosphorylation of SAPK/JNK, ERK1/2, and p38, as well as p65/RelA, was higher in HIV-1–infected macrophages than in noninfected cells, despite the relatively low rate of infection of primary human macrophages by WT viruses (between 10% and 40%; Fig. 1, A–D). After stimulation of FcR, however, the phosphorylation of ERK1/2 was markedly reduced in HIV-1–infected macrophages compared with noninfected cells (Fig. 1, E and F). Quantification of the results indicated that there are two waves of activation of ERK1/2 in control cells with peaks at 10 and 180 min, but no increase in ERK1/2 phosphorylation in HIV-infected macrophages. This was specific to the HIV-1 viral infection, because we did not observe the same defects after other preactivation treatments (Fig. 1 G).

When we used a cytokine array to detect various cytokines and chemokines in a semiquantitative manner in the supernatant of cells 6 h after stimulation (Fig. 1 H), we also noticed reduced production of cytokines in the supernatant of cells preinfected with HIV-1_{ADA}WT, both in resting conditions and after a phagocytic stimulus, compared with noninfected cells. Therefore, our results indicate that the HIV-1 infection of macrophages induced a basal "preactivation" of the cells that dampened the cellular response downstream of the engagement of the phagocytic receptors.

Phagocytosis eventually leads to the degradation of the ingested material. Some pathogens, such as *Salmonella typhimurium*, are invasive facultative intracellular bacteria that have evolved highly adapted gene expression programs to shape the vacuole in which they reside. We compared the intracellular survival of *S. typhimurium* in HIV-$1_{ADA\text{-}VSV\text{-}G}$WT–infected versus noninfected macrophages using a gentamicin-plating assay (Fig. 1 I). A VSV-G pseudotyped virus was used to achieve higher rates of infection and the bacterial survival was assessed by counting the number of intracellular bacteria 1 and 24 h postincubation. The data are expressed as a ratio (i.e., index of survival, expressed relative to noninfected macrophages). Intracellular *S. typhimurium* survived 3.2-fold ± 0.2-fold better in HIV-infected macrophages compared with control cells. Such a defect in bacterial clearance is indicative of an altered phagosomal maturation.

HIV infection impairs phagosome maturation

To further characterize the defective clearance activity in macrophages infected with HIV-1, we analyzed the late steps of phagosome maturation and the luminal content of phagosomes using 3-µm beads coated with IgG to target FcRs. These beads were coupled to fluorophores sensitive to the hydrolytic activity (DQ-BSA beads) or to the oxidative burst (dichlorodihydrofluorescein diacetate [H_2DCFDA]-OxyBURST beads), as well as a pH-insensitive calibration fluorophore to correct for variation in phagocytosis (Yates and Russell, 2008; Podinovskaia et al., 2013). MDMs infected with HIV-$1_{ADA\text{-}VSV\text{-}G}$WT or noninfected controls were incubated for various times at 37°C with beads and then analyzed by flow cytometry focusing on the population of cells associated with beads (Fig. 2, A–D). The oxidative burst was detected as soon as 20–30 min until 3 h after contact with the beads in noninfected MDMs. In HIV-1–infected macrophages, the signal was reduced at each time point, up to 92% of the control condition (Fig. 2 C). The hydrolytic activity was detectable after 1.5 h of contact with beads in control conditions. In HIV-infected macrophages, we observed that the hydrolytic activity was reduced compared with noninfected MDMs (between 23% and 80% depending on the time; Fig. 2 D). Therefore, there is a marked decrease in the production of reactive oxygen species and hydrolytic activity in phagosomes of HIV-1–infected macrophages.

HIV_{ADA}WT-infected macrophages were then allowed to phagocytose IgG-opsonized SRBCs for various times before fixation, permeabilization, and labeling with anti-LAMP1 (Fig. 2, E–G), a marker of late endosomes/lysosomes (Scott et al., 2014), and anti-p24 antibodies to detect HIV-1–infected cells. As shown in Fig. 2 G, although the majority of internalized SRBCs were surrounded by a relatively continuous LAMP1 staining in noninfected macrophages after 20 min or 60 min, LAMP1 staining of phagosomes in HIV-infected macrophages was often absent or was present as scattered staining around the SRBCs (Fig. 2 G, arrows), which was not scored as a positive recruitment. Accordingly, the recruitment of LAMP1, scored on internalized phagosomes only to rule out the known effect of HIV-1 infection on the efficiency of phagosome formation (Mazzolini et al., 2010), was inhibited by 24%–64%

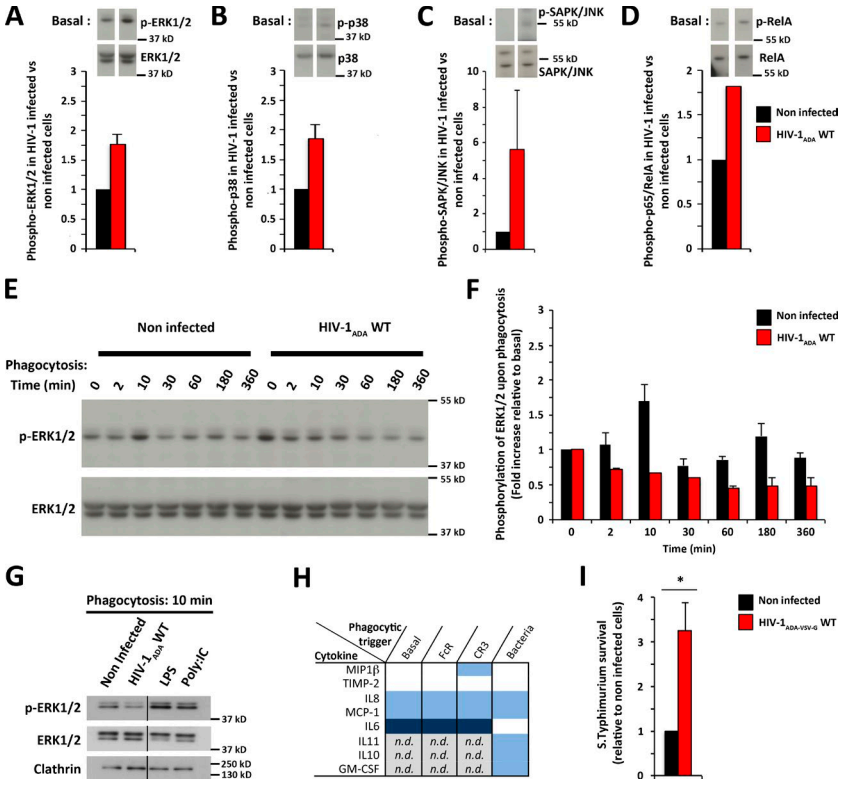

Figure 1. **Activation status, signaling response to phagocytic triggers, and bacterial clearance in HIV-1–infected macrophages.** (A–D) Primary human macrophages were noninfected or infected with HIV-1_{ADA}WT for 8 d. Total lysates were subjected to Western blotting with anti–phospho-ERK1/2 (A), anti–phospho-p38 (B), anti–phospho-SAPK/JNK (C), and anti–phospho-p65/RelA (D). The chemiluminescent signal was quantified and expressed as related to the noninfected condition, showing basal activation by HIV infection. (E) Macrophages infected for 8 d were incubated for different times with IgG-SRBCs at 37°C and then analyzed by Western blotting with anti–phospho ERK1/2 and anti–ERK1/2. (F) Results are expressed as a fold increase related to the basal condition for noninfected or HIV-1–infected cells. Means ± SEM of three different experiments are plotted. (G) Primary human macrophages were noninfected, infected with HIV-1_{ADA}WT, or treated with lipopolysaccharide (LPS) or polyinosinic:polycytidylic acid (Poly:IC) for 8 d. The cells were then incubated for different times with IgG-SRBCs at 37°C and then analyzed by Western blotting with anti–phospho-ERK1/2, anti-ERK1/2, or anti-clathrin as a loading control. One of three representative experiments is presented. (H) Human macrophages were infected with HIV-1_{ADA} WT or mock infected for 8 d. They were incubated or not (basal) with IgG-SRBCs (FcR), with complement-SRBCs (CR3), or with invasive *S. typhimurium* for 6 h at 37°C. Supernatants were collected and analyzed on human cytokine antibody arrays. Semiquantitative analysis was performed and the results are presented as a table, with white indicating no differential expression compared with noninfected conditions, light blue indicating down-regulation, and dark blue indicating higher down-regulation. n.d., not detected in control as well as HIV-infected conditions. Three independent experiments were performed with similar results. (I) The number of intracellular *S. typhimurium* at 24 h was divided by the number of bacteria at 1 h in HIV-1–infected or noninfected macrophages and results are expressed as related to noninfected cells. The mean ± SEM of four independent experiments is presented. *, $P < 0.05$.

depending on the time point analyzed (Fig. 2, E and F). The recruitment of LAMP1 on phagosomes of p24-negative cells of the same coverslips in HIV-1–infected conditions was not inhibited, indicating that there was no bystander effect in neighboring p24-negative cells (unpublished data).

Together, these results indicate that phagosome maturation, as defined by the acquisition of lysosomal markers, hydrolytic activity, and the superoxide burst, is impaired in HIV-1 WT–infected macrophages.

Hijacking of the MICAL-L1/EHD3 endosomal sorting machinery in HIV-infected macrophages

To better identify where phagosome maturation is arrested, we stained cells for the early endosomal marker EEA1 (Fig. 3 A). We observed that its recruitment was not modified in HIV-infected macrophages, with this marker being lost progressively after 10–20 min (Fig. 3 A). Therefore, the maturation arrest is between early and late endosomal marker acquisition. We investigated the localization of the MICAL-L1 protein and its partner the C-terminal Eps15 homology domain EHD ATPase protein 3 (EHD3), involved in control and tubulation on sorting/recycling endosomes (Fig. 3, B and C; Abou-Zeid et al., 2011; Cai et al., 2013). MICAL-L1 distribution was modified in HIV_{ADA}WT-infected macrophages, in which more tubules were observed compared with noninfected macrophages (Fig. 3 B). Analysis of optical sections showed that EHD3 localization was also modified and that it was recruited to virus-containing compartments (Fig. 3 C). Because the functions of MICAL-L1 and EHD3 in phagosome maturation had not been reported before, we knocked down their expression in MDMs and observed a 41 ± 8% and 39 ± 7% defect, respectively, in the recruitment of LAMP1 calculated on internalized phagosomes after 1 h of phagocytosis (Fig. 3, D and E; $P < 0.05$).

Together, these results point to a defect in phagosome maturation at the level of sorting/recycling endosomes with hijacking of the EHD3/MICAL-L1 sorting machinery by HIV-1.

The perturbation of phagosome maturation in macrophages requires established infection and expression of the viral factor Vpr

To better understand how HIV perturbs the functions of macrophages, we infected the primary human macrophages with HIV-1_{ADA}WT for various times before assessing LAMP1 recruitment as in Fig. 2. There was no significant inhibition of phagosomal maturation after 2 or 3 d (Fig. 4 A). However, we observed a marked inhibition of the recruitment of LAMP1 on the phagosomes after 6 or 8 d of HIV infection. Moreover, the inhibition of phagosomal maturation by HIV-1 was not observed when

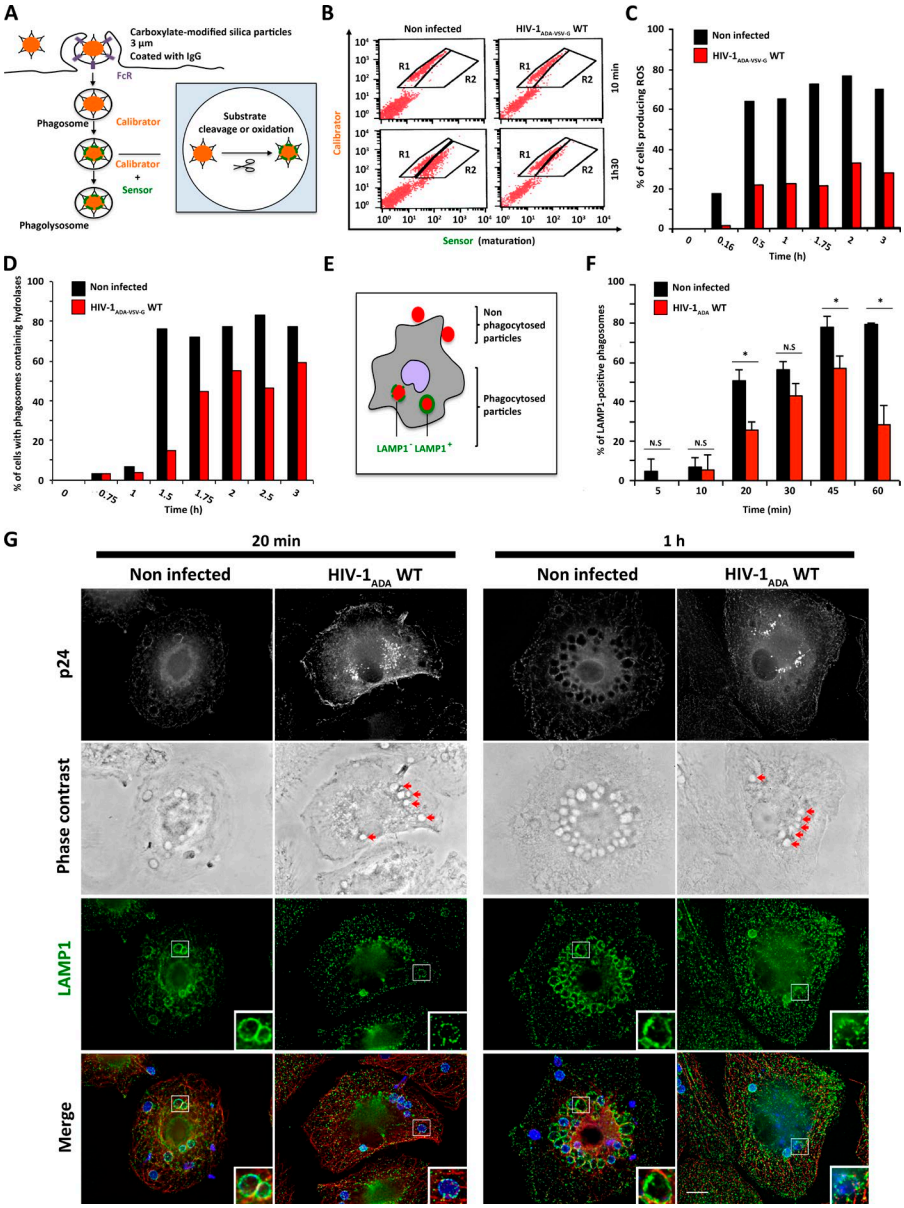

Figure 2. **HIV-1 infection of macrophages inhibits phagosomal hydrolytic and oxidative activity and induces a delay in the recruitment of late endocytic markers on phagosomes.** Primary human macrophages were infected with HIV-1_{ADA}-VSV-G-WT or mock infected for 8 d before incubation with IgG-opsonized beads for various times. (A) Schematic representation of the detection of hydrolytic activity with DQ-BSA beads and oxidative activity with H_2DCF DA-OxyBURST beads. Modified substrates emit at 520 nm (sensor) and calibration fluorochrome emits at 647 nm (calibrator). (B) At different times of incubation, cells were placed on ice, resuspended with cold PBS, fixed, and analyzed by flow cytometry. The number of cells containing beads with a modified sensor fluorescence (R2) was divided by the total number of cells containing beads (positive for calibrator, y axis, R1 + R2). (C and D) Results are expressed as a percentage of cells with phagosomes containing detected oxidative (C) or hydrolytic (D) activity. One representative experiment of at least three is shown (see also Fig. S1). (E–G) Primary human macrophages were infected with HIV-1_{ADA} WT or mock infected for 8 d. The cells were incubated for different times with IgG-SRBCs at 37°C. Macrophages were fixed, permeabilized, and labeled with AMCA-labeled anti–rabbit IgG to detect the total SRBCs (unpublished data), anti-p24 followed by Cy2-labeled anti–goat IgG (top line), anti-LAMP1 (third line) followed by Cy3-labeled anti–mouse IgG, and anti-tubulin followed by Cy5-labeled anti–human IgG (not depicted). Particles internalized in phagosomes are also detectable by phase contrast (second row, red arrows). Merged images (bottom line) show SRBCs in blue, LAMP1 in green, and microtubules in red. Z-stacks of wide-field fluorescent images were acquired, deconvoluted, and treated with ImageJ. Bar, 10 µm; magnification in insets is 2.1× (G). The number of phagosomes positive or negative for LAMP1 was counted for at least 10 cells per condition (E and F). Results are expressed as a percentage of total internal phagosome number ± SEM (>200 phagosomes per condition, repeated in $n = 3$ independent experiments on different donors). *, $P < 0.05$.

macrophages were treated with integrase inhibitor raltegravir, indicating that viral integration was necessary (Fig. 4 B). The capacity of macrophages to ingest IgG-opsonized particles, on the other hand, was progressively reduced with time of infection (Fig. 4 C); using *nef*-deleted HIV-1 variants, we confirmed that Nef was important for the internalization step (Fig. 4, C and F; Mazzolini et al., 2010). In contrast, Nef was not significantly involved in inhibiting recruitment of LAMP1 on the phagosomes that still did get internalized (Fig. 4 D). Most importantly, infection of macrophages with an HIV-1 strain deleted for the Vpr factor showed a recovery of the recruitment of LAMP1 on phagosomes, indicating that Vpr was essential for the virus to inhibit phagosome maturation (Fig. 4 E). Interestingly, there was no difference between HIV-$_{YU\text{-}2}$WT and HIV-$_{YU\text{-}2}\Delta$Vpr on the efficiency of the internalization step of phagocytosis (Fig. 4 G), demonstrating that, unlike Nef, Vpr is not involved in phagosome formation but is involved in phagosome maturation.

Together, these data clearly demonstrate that the impairment of phagosome maturation in human macrophages is not a consequence of the perturbation of Nef-dependent early membrane remodeling events. Moreover, they reveal that the virus evolved with two factors to inhibit entry and maturation. Thus, Vpr was identified as a major regulator of phagosome maturation in HIV-infected macrophages.

The centripetal movement of phagosomes is slower in HIV-infected macrophages in a Vpr-dependent manner

Next, we investigated the subcellular localization of phagosomes containing IgG-opsonized SRBCs after uptake (Fig. 5, A and B). In control macrophages, ≈70% of phagosomes reached the cell center within 20 min and ≈90% after 60 min, whereas only 30% of the phagosomes were at the cell center in HIV-infected macrophages after 20 min and 44% after 60 min, with much variability. The movement of the phagosomes to the cell center was delayed in macrophages infected with HIV-1_{ADA} WT, and this delay was at least partially dependent on Vpr because the phagosome distribution was not significantly different between cells infected with HIV-$_{YU\text{-}2}\Delta$Vpr and noninfected macrophages (Fig. 5 C; $P < 0.05$).

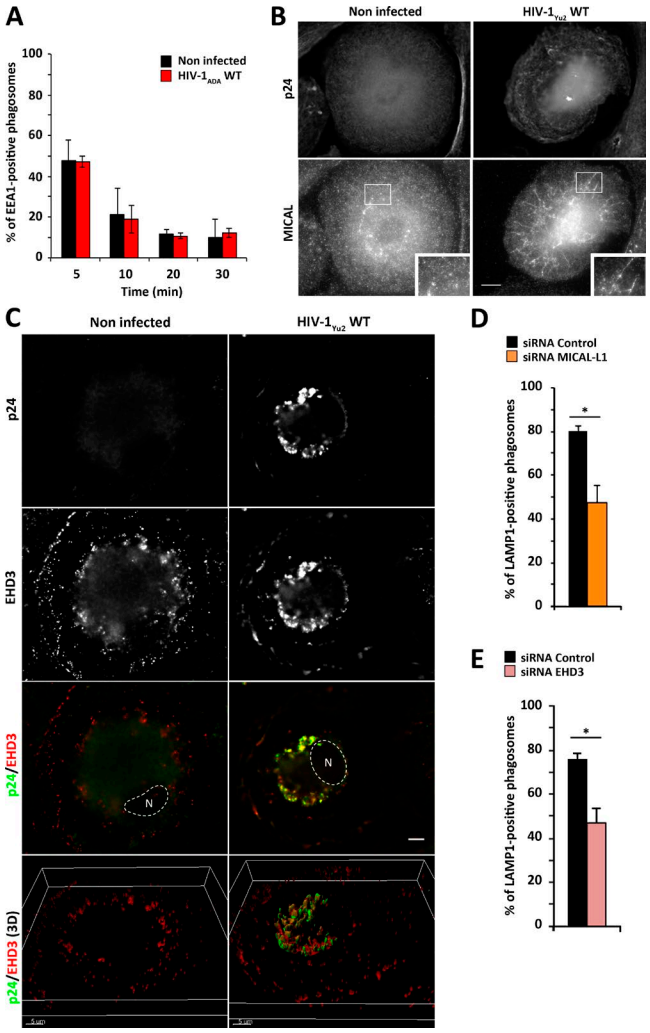

Figure 3. **HIV-1 perturbs and hijacks the EHD3/MICAL-L1 sorting machinery.** (A) Primary human macrophages were infected with HIV-1_{ADA} WT or mock infected for 8 d. The cells were incubated for different times with IgG-SRBCs at 37°C. Macrophages were treated as in Fig. 2 F except that staining was with anti-EEA1 followed by Cy3-labeled anti–mouse IgG. The number of internal phagosomes positive for EEA1 was counted. Results are expressed as a percentage of total internal phagosome number ± SEM (>200 phagosomes per condition, repeated in $n = 3$ independent experiments on different donors). (B) Primary human macrophages were noninfected (left) or infected with HIV-1_{YU-2}WT (right) for 8 d. The cells were then fixed and stained with an anti–p24 antibody, followed by Alexa Fluor 488–coupled anti–goat IgG (top panels) and an anti–MICAL-L1 (B) or anti-EHD3 (C) antibody, followed by Cy3-labeled anti–rabbit IgG and Cy3-labeled anti–mouse IgG, respectively. Stacks of images were acquired and a maximum-intensity projection is shown in B. Bar, 5 µm; magnification in insets is 2×. (C) Stacks were deconvoluted and single optical sections are shown. 3D reconstitution was performed with Imaris. N, nucleus. Bar, 5 µm. (D and E) Macrophages differentiated for 5 d were treated with control siRNA or siRNA against MICAL-L1 (D) or siRNA against EHD3 (E) for 72 h. They were then allowed to phagocytose IgG-opsonized SRBCs for 1h, fixed, and stained to detect SRBCs with Alexa Fluor 647–coupled anti–rabbit IgG and LAMP1 with anti-LAMP1 followed by Cy3-labeled anti–mouse IgG (not depicted). LAMP1 acquisition was quantified as in Fig. 2. Results are expressed as a percentage of control cells. The means ± SEM of three independent experiments (donors) are plotted. *, $P < 0.05$.

To further characterize the centripetal movement of phagosomes, we followed their movement in living HIV-1–infected macrophages (Fig. 5, D and E) using a spinning disk confocal microscope and HIV-1Gag-iGFP, which generates infectious virions in primary macrophages (Koppensteiner et al., 2012a; Gaudin et al., 2013). Phagosome movements were recorded every minute for 2 h after uptake, the internalization of particles being detected via a transition from bright phase to dark phase. The recorded velocities are of similar magnitude to the speeds already reported (Blocker et al., 1998; Harrison et al., 2003). The movements were slower in HIV-infected macrophages immediately after uptake (Fig. 5, C and D). Therefore, the peripheral location of phagosomes in HIV-infected macrophages appears as a consequence of a slowdown in the intracellular trafficking of the newly formed phagosomes.

Perturbed localization at microtubule plus ends of EB1 and p150^{Glued} in HIV-infected macrophages

Because phagosome movement is a microtubule-dependent process (Blocker et al., 1998; Harrison et al., 2003), we investigated the microtubule network in HIV-1–infected macrophages (Fig. 6). Control MDMs and cells infected with HIV-$_{YU-2}$WT or HIV-$_{YU-2}$ΔVpr for 8 d were treated with nocodazole to depolymerize the microtubules (Fig. 6 A). After extensive washes, the cells were placed in medium without nocodazole to allow microtubule repolymerization. Although there was no striking difference between HIV-1–infected or control cells in steady-state conditions (basal), microtubule repolymerization was slower in HIV-1–infected MDMs compared with noninfected cells. The phenotype was intermediate in MDMs infected with a *vpr-deleted* HIV-1 mutant. Therefore, the infection of macrophages with HIV-1 perturbs the microtubule dynamics.

Proteins that localize to growing microtubule plus ends, collectively called plus-end tracking proteins (+TIPs), such as EB1 (Akhmanova and Steinmetz, 2010; Gouveia and Akhmanova, 2010), are important to stabilize microtubules and confer local functions of the microtubule cytoskeleton. We observed a reduced localization of EB1-positive comet-shaped structures at the periphery of the cells in HIV-1–infected macrophages (Fig. 6 C), although the total amount of EB1 was unchanged (Fig. 6 D). There was no such reduction in HIV-ΔVpr–infected cells (Fig. 6 D). The centripetal movement of organelles relies on the dynein/dynactin motor complex (Harrison et al., 2003) and EB1 was recently shown in vitro to recruit p150^{Glued} to target the dynein/dynactin complex to the plus ends of microtubules (Duellberg et al., 2014). We observed that p150^{Glued} was also mislocalized in HIV-infected macrophages (Fig. 6 E) and that the effect was partial in HIV-ΔVpr–infected cells.

Collectively, our data show that HIV-1 infection affects the plus end loading of EB1 and p150^{Glued} in a Vpr-dependent manner in primary human macrophages.

Vpr is sufficient to interact with and perturb the localization of EB1, p150^{Glued}, and DHC

To analyze whether the expression of Vpr alone induces the mislocalization of +TIPs, we transiently transfected primary human macrophages to express HA-Vpr and stained them for EB1 (Fig. 7, A and B) and p150^{Glued} (Fig. 7, C and D). Confocal sections and 3D reconstructions show that expression of Vpr led to the mislocalization of EB1 and p150^{Glued} from the plus ends of microtubules to more perinuclear and also nuclear localization where Vpr is accumulated in these conditions.

To further confirm the interaction between Vpr and microtubule-associated proteins, we performed coimmunopre-

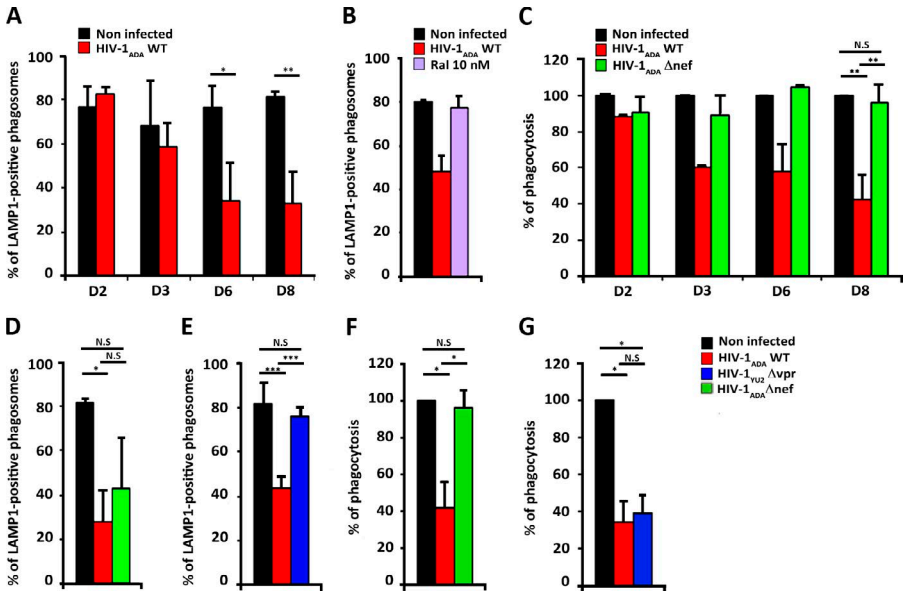

Figure 4. **Established HIV-1 infection and the viral factor Vpr are important for the phagosome maturation defect.** (A) Primary human macrophages were noninfected (black bars) or infected with HIV-1_{ADA} WT (red bars) for 2, 3, 6, or 8 d. At each time point, the cells were incubated for 1 h with IgG-SRBCs at 37°C, fixed, and permeabilized. Then, they were labeled with Cy5-labeled anti–rabbit IgG to detect the total SRBCs, an anti-p24 antibody followed by Cy2-labeled anti–goat IgG to detect the infected cells, and an anti–LAMP1, followed by Cy3-labeled anti–mouse IgG. Z-stacks of fluorescence images were acquired and analyzed with ImageJ. The number of phagosomes positive for LAMP1 was calculated for >200 phagosomes per condition at each time point. Results are expressed as a percentage of total phagosomes. The means ± SEM from two independent experiments are plotted. (B) Primary human macrophages were noninfected (black bars), infected with HIV-1_{ADA} WT alone (red bars), or in the presence of raltegravir (violet bars) at 10 mM for 8 d. Data were analyzed as in A. (C) Primary human macrophages were noninfected or infected with HIV-1_{ADA}WT or HIV-1_{ADA}ΔNef for 2, 3, 6, or 8 d. At each time point, the cells were incubated for 1 h with IgG-SRBCs at 37°C and fixed. External and internal SRBCs were counted and the efficiency of phagocytosis was calculated for noninfected cells (black bars), HIV-1_{ADA}WT–infected cells (red bars), and HIV-1_{ADA}ΔNef–infected cells (green bars). Results are expressed as a percentage of control noninfected cells. The means ± SEM of three independent experiments are plotted. (D and F) Primary human macrophages were noninfected (black bars) or infected with HIV-1_{ADA}WT (red bars) or HIV-1_{ADA}ΔNef (green bars) for 8 d. Cells were treated and results analyzed as in A and C, respectively. The means ± SEM from five independent experiments are plotted. (E and G) Primary human macrophages were noninfected (black bars) or infected with HIV-1_{YU-2}WT (red bars) or HIV-1_{YU-2}ΔVpr (blue bars) for 8 d. Cells were treated and results analyzed as in A and C, respectively. The means ± SEM from five independent experiments are plotted. *, P < 0.05; **, P < 0.005.

cipitation experiments to precipitate HA-Vpr and mass spectrometry analysis on lysates from transfected HeLa cells. We found that DHC was part of the proteins precipitated with HA-Vpr but not after control transfection with the empty HA plasmid. We confirmed this result by Western blotting (Fig. 7 E).

Next, we used the proximity ligation in situ assay (Duolink; Söderberg et al., 2006) to assess protein interaction (Fig. 7, F–K). For this, we used HeLa cells with conditions to avoid massive toxic overexpression of HA-Vpr but reaching around 30% transfection efficiency. The mean number of spots detected per cell randomly analyzed on microscopy fields showed that Vpr interacted with EB1, $p150^{Glued}$, and DHC (Fig. 7, H–K), compared with negative controls obtained by omitting one primary antibody in HA-Vpr–expressing coverslips

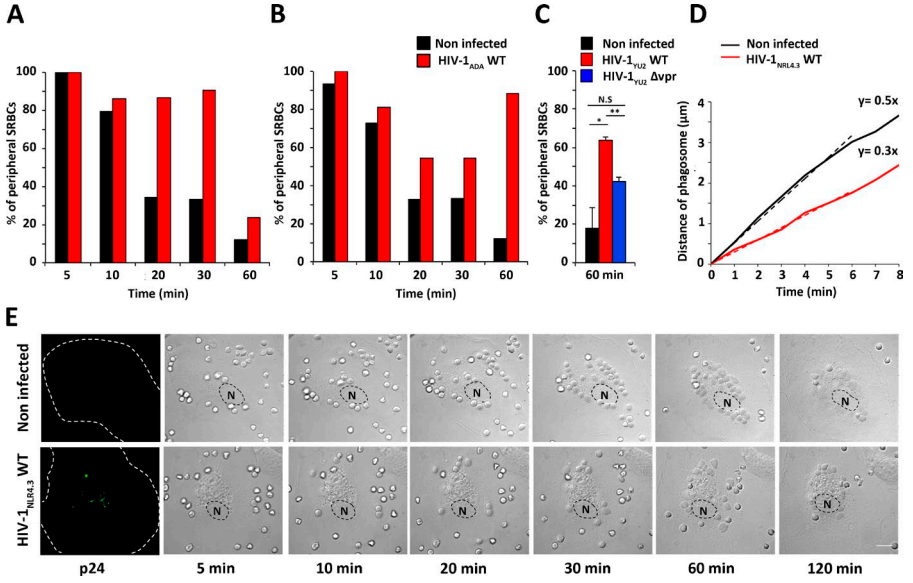

Figure 5. **Centripetal movement of phagosomes is inhibited in HIV-1–infected macrophages.** (A and B) Primary human macrophages were noninfected (black bars) or infected with HIV-1_{ADA}WT (red bars) for 8 d. The cells were incubated for different time points with IgG-SRBCs at 37°C and then fixed and permeabilized. They were labeled and analyzed as described in Fig. 2. Peripheral SRBCs, situated at a distance to the nucleus of more than two SRBCs in diameter, were counted for at least 200 phagosomes per condition at each time point. Results are expressed as the percentage of total number of SRBCs; two independent experiments on different donors are shown. (C) Primary human macrophages were noninfected (black bars) or infected with HIV-1_{YU-2}WT (red bars) or HIV-1_{YU-2}ΔVpr (blue bars) for 8 d. Cells were incubated with IgG-SRBCs for 1 h at 37°C and then analyzed as in A. The means ± SEM of three independent experiments are plotted. (D) Primary human macrophages were infected with HIV-1Gag-iGFP for 8 d, then incubated with IgG-SRBCs at 37°C under a spinning disk confocal microscope equipped with 5% CO_2 and a heated chamber. Images were recorded every minute for 120 min. The distances covered by internal phagosomes were measured for 53 phagosomes in noninfected cells and 60 phagosomes in HIV-infected macrophages and were plotted against time. The speed was calculated by linear regression. (E) Primary human macrophages were treated as in C. Gallery of phase contrast images of noninfected (top panels; see also Video 1) and HIV-1Gag-iGFP–infected (bottom panels; see also Video 2) cells showing phagosome movement. Bar, 10 µm. *, P < 0.05; **, P < 0.005.

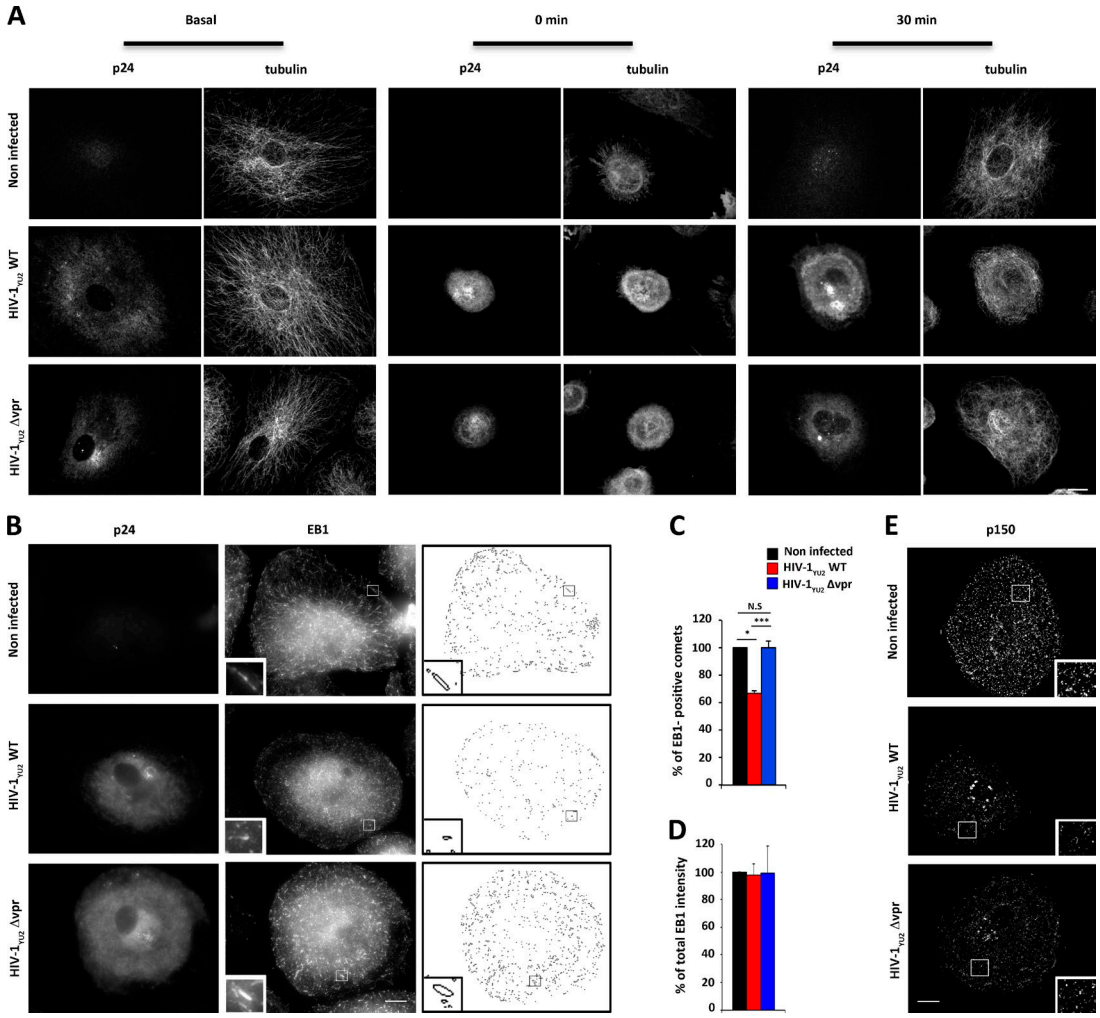

Figure 6. **HIV-1 and Vpr perturb the microtubule dynamics and localization of EB1 and p150^{Glued}.** (A) Primary human macrophages were noninfected (top), infected with HIV-1$_{YU-2}$WT (middle), or infected with HIV-1$_{YU-2}$ΔVpr (bottom) for 8 d. Cells were treated or not (basal) with nocodazole at 10 µM for 1 h at 37°C. After washing, cells were fixed (time 0) or incubated at 37°C without nocodazole for the indicated times before fixation. Macrophages were then labeled with an anti-p24 antibody, followed by Cy2-labeled anti–mouse IgG and a recombinant anti-tubulin, and then followed by Cy3-labeled anti–human IgG. Images were acquired under a spinning disk microscope. One optical section for tubulin and Z projections of sections for p24 staining, from stacks of representative cells, are shown. Bar, 10 µm. (B) Primary human macrophages were noninfected (top), infected with HIV-1$_{YU-2}$WT (middle), or infected with HIV-1$_{YU-2}$ΔVpr (bottom) for 8 d. The cells were then fixed and stained with an anti-p24, followed by Cy2-labeled anti–goat IgG (left) and an anti-EB1, followed by Cy3-labeled anti–mouse IgG (middle). Stacks of images were acquired with a wide-field microscope and analyzed to define (right) and quantify (C) the comet-shaped ellipsoid objects. Bar, 5 µm; magnification in insets is 3.3×. (C and D) Macrophages were treated as in B and the number of EB1-positive comets (C; n > 2000 comets per condition) or the total intensity of EB1 staining (D) was calculated in 12 noninfected (black bars), 12 HIV-1$_{YU-2}$WT–infected (red bars), and 12 HIV-1$_{YU-2}$ΔVpr (blue bars) cells. Results are expressed as a percentage of control noninfected cells. The means ± SEM of three independent experiments (donors) are plotted. (E) Primary human macrophages were noninfected (top), infected with HIV-1$_{YU-2}$WT (middle), or infected HIV-1$_{YU-2}$ΔVpr (bottom) for 8 d. The cells were then fixed and stained with an anti-p24 antibody, followed by Cy2-labeled anti–goat IgG (not depicted) and an anti-p150^{Glued}, followed by Cy3-labeled anti–mouse IgG. Stack of images were acquired, and Z projection of images is shown after TopHatFilter treatment. Bar, 10 µm; magnification in insets is 2.2×. *, P < 0.05; ***, P < 0.0005.

(Fig. 7 F) or with the results obtained after empty HA plasmid transfection or a positive control combining the detection of α-tubulin and DHC.

In conclusion, Vpr interacted with EB1, p150^{Glued}, and DHC and is sufficient to induce their mislocalization.

Vpr is sufficient to impair phagosome maturation

When human macrophages transiently expressing HA-Vpr were allowed to phagocytose IgG-opsonized SRBCs, we observed that Vpr led to a significant inhibition of LAMP1 recruitment on internalized phagosomes (Fig. 8, A and B), indicating that expression of Vpr alone was sufficient to alter the recruitment of this late phagosomal marker. In addition, the depletion of EB1 induced a 38.1% ± 4.5% defect in phagosome maturation, as measured with the acquisition of LAMP1 on internalized phagosomes (Fig. 8, C and D). Together, these results show that EB1 depletion or Vpr expression was sufficient to lead to a defect in phagosome maturation.

Discussion

In this study, we report that HIV-1–infected human macrophages show profound alterations of their functions leading to impairment of bacterial clearance. Importantly, we found that

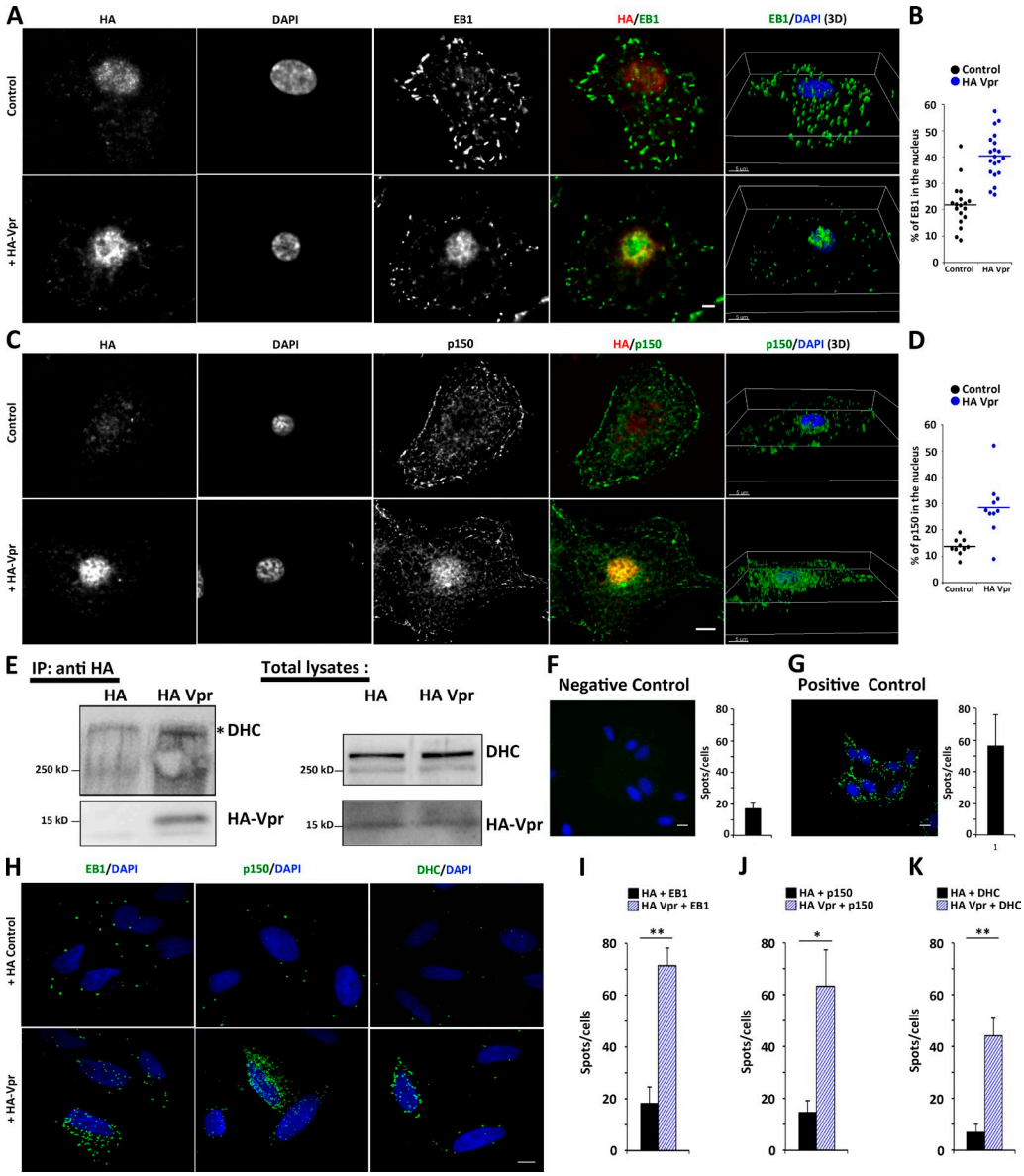

Figure 7. **Vpr expression perturbs EB1 and p150^{Glued} localization, leading to a phagosome maturation defect.** (A) MDMs were nucleofected at day 5 of differentiation to express HA-Vpr or with the HA plasmid as a control. 5 h later, they were fixed and stained with anti-HA antibodies followed by Cy3-labeled anti–rat IgG (left), DAPI (second lane), and an anti-EB1, followed by Alexa Fluor 488–coupled anti–mouse IgG (middle). Stack of images were acquired and one optical deconvoluted section is shown. Combined images and a 3D reconstitution are shown (right). Bar, 10 µm. (B) Cells were treated as in A and the percentage of EB1 staining localized in the nucleus as detected with the DAPI staining was calculated using Icy software for HA-Vpr–expressing cells and control cells. The dot plot shows the results and means ± SEM from 20 cells of two independent experiments (donors). (C and D) MDMs were nucleofected and treated as in A and B except that p150^{Glued} was stained. Bar, 10 µm. The dot plot shows the results and means ± SEM from 10 cells of one experiment. (E) HeLa cells were transiently transfected to express HA-Vpr or with the HA plasmid as a control. Immunoprecipitation with anti-HA antibodies revealed coimmunoprecipitation of endogenous DHC detected with anti-DHC antibodies. The amounts of total proteins in lysates (1% of total lysates) are shown (right panels). Three independent experiments were performed. (F–K) HeLa cells were transiently transfected to express HA-Vpr or with the HA plasmid as a control, then fixed, and the Duolink proximity ligation in situ assay technology was used with rabbit anti–HA antibodies to detect Vpr combined with mouse mAb anti–EB1 (left panels and I) or mouse anti–p150^{Glued} (middle panels and J), or with mouse anti–HA to detect Vpr combined with rabbit anti–DHC (right panels and K) (H). Negative control was obtained by omitting anti-HA antibody with mouse anti–p150^{Glued} (F) and positive control was with mouse mAb anti–tubulin and rabbit anti–DHC (G). Bars, 10 µm. The number of fluorescent spots was automatically counted using the Icy software SpotDetector function, and the mean number of spots per cell based on nuclei counting in different microscopy fields was plotted (F, G, and I–K). The means ± SEM from three independent experiments are plotted. *, $P < 0.05$; **, $P < 0.005$.

the Vpr viral factor was responsible for defects in phagosome maturation, and we showed for the first time that it affects microtubule-dependent trafficking and thus endocytic events.

We demonstrated that the maturation of phagosomes into phagolysosomes was impaired in HIV-infected macrophages. This maturation process is complex and incorporates a wide range of biological activities, including the intraphagosomal superoxide burst, the degree of acidification, the extent of phagosome–lysosome fusion, and proteolytic capacity of lysosomes (Russell and Yates, 2007; Botelho and Grinstein, 2011; Fairn and Grinstein, 2012; Flannagan et al., 2012). Because activation of murine bone marrow–derived macrophages was described to modify the early phagosomal degradative capacities (Yates et al., 2007), impairment of phagosomal maturation in HIV-infected

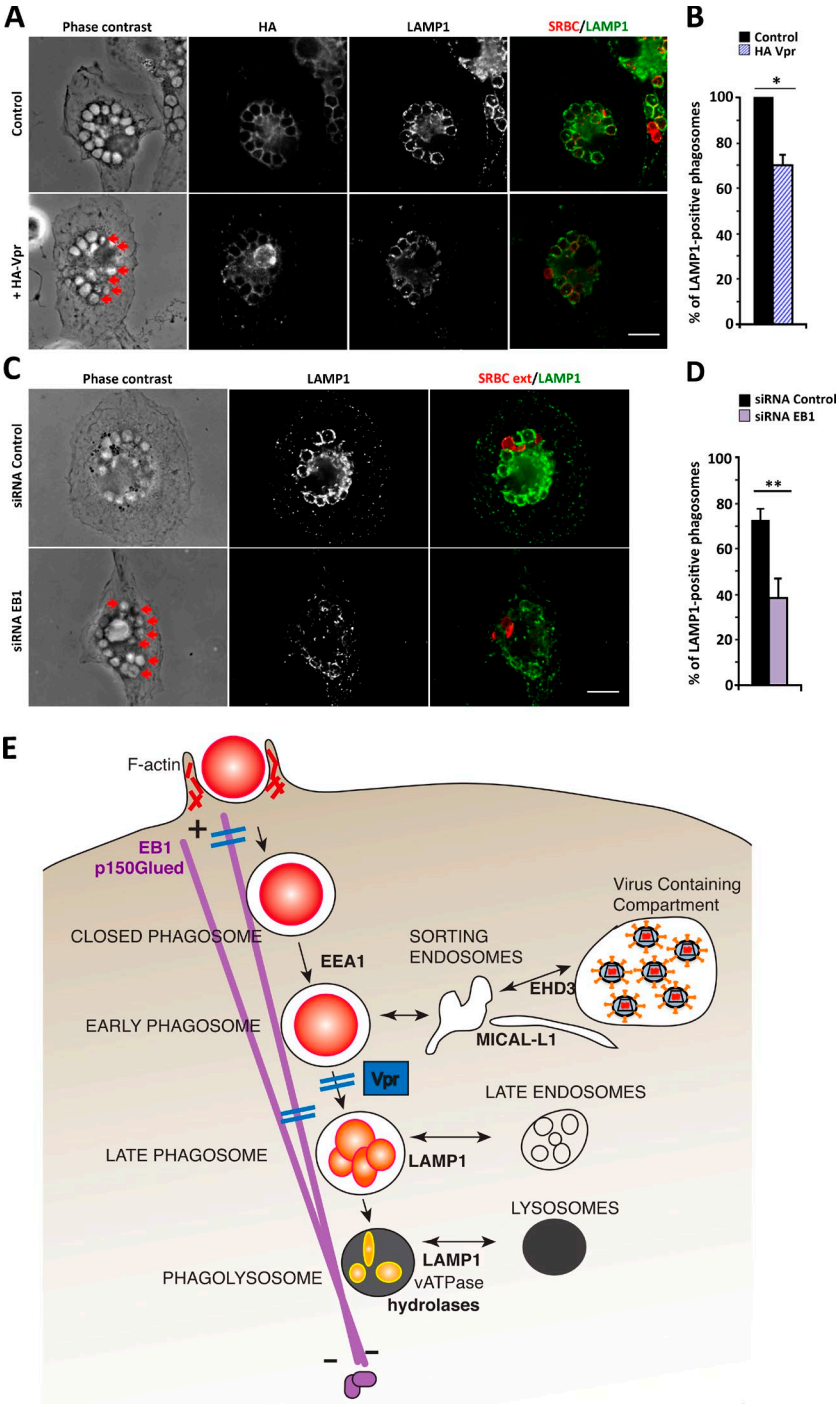

Figure 8. **Vpr expression or EB1 depletion leads to defective phagosome maturation.** (A) MDMs were nucleofected at day 5 of differentiation to express HA-Vpr or with the HA plasmid as a control, incubated for 60 min with IgG-SRBCs at 37°C, and then fixed and permeabilized. They were labeled and analyzed as described in Fig. 2 (E and F). Z-stacks of wide-field fluorescent images were acquired and deconvoluted and a Z projection (ImageJ) is shown. Bar, 10 µm. (B) The number of LAMP1-positive phagosomes was counted as in Fig. 2 and expressed as a percentage of control HA-negative cells. The means ± SEM of three independent experiments are plotted ($P < 0.05$). (C) MDMs differentiated for 5 d were treated with control siRNA or siRNA against EB1 for 72 h. They were then allowed to phagocytose IgG-opsonized SRBCs for 1 h, fixed, and stained to detect SRBCs with Alexa Fluor–coupled anti–rabbit IgG (not depicted, red in the merge images, right panels) and LAMP1 with anti-LAMP1 followed by Cy3-labeled anti–mouse IgG (middle panels). SRBCs are also detected with phase contrast (left panels). Z-stacks of wide-field fluorescent images were acquired and deconvoluted and a Z projection (ImageJ) is shown. Bar, 10 µm. (D) LAMP1 acquisition was quantified as in Fig. 2. Results are expressed as a percentage of control cells. The means ± SEM of three independent experiments are plotted ($P < 0.05$). (E) Model of Vpr-induced microtubule-dependent trafficking defects. Phagosome formation is partially inhibited by HIV Nef, perturbing the focal membrane remodeling. Phagosomes that do form in HIV-1–infected macrophages do not move efficiently onto the microtubules to reach the cell center and to undergo maturation. They show altered sorting events that are a consequence of the hijacking of the EHD3 and MICAL-L1 components of the sorting machinery. This is caused by impaired plus end loading of $p150^{Glued}$ by EB1, which is mislocalized by Vpr. Vpr expression or EB1 depletion is sufficient to recapitulate these events. *, $P < 0.05$; **, $P < 0.005$.

macrophages could be linked to the preactivated status that we observed. Activation of macrophages as well as HIV infection was previously reported to induce stabilization of the microtubule network (Patel et al., 2009; Sabo et al., 2013), but the phagosomal defect that we described seems to be specific to an established HIV-1 viral infection, because we did not observe the same defects after other treatments. Of note, the viral-containing compartment was shown to be less acidic than late endosomes in human macrophages (Jouve et al., 2007). We did not observe a massive colocalization of the viral capsid and the phagosomal content; therefore, the defect in phagosomal maturation that we describe does not seem to be related to the presence of the virus within the phagosome.

The perturbation of phagosomal maturation described here requires the establishment of a complete viral cycle. Importantly, the defects in phagosome formation (Mazzolini et al., 2010) and in phagosome maturation (this study) clearly rely on different steps of the viral cycle and different viral factors. This correlates with the temporal expression of the two proteins, because Nef is expressed abundantly early during virus replication, whereas Vpr is expressed later (Planelles and Benichou, 2009; Witkowski and Verhasselt, 2013; Guenzel et al., 2014). The effects on late events of phagosome maturation and activation are not a consequence of Nef's known ability to partially inhibit the phagosome formation in HIV-1–infected macrophages (Mazzolini et al., 2010) and to modify intracellular

trafficking and signaling (Fackler and Baur, 2002; Foster and Garcia, 2008; Witkowski and Verhasselt, 2013). Strikingly, we show that Vpr affects microtubule-dependent intracellular trafficking, and thus normal phagolysosome biogenesis. Vpr is a small basic protein conserved among human HIV-1 and HIV-2 and simian immunodeficiency virus. It regulates cell cycle progression, reverse transcription, and viral DNA nuclear import (McDonald et al., 2002; Planelles and Benichou, 2009; Kogan and Rappaport, 2011; Strebel, 2013; Guenzel et al., 2014). Therefore, our results reveal an unexpected role of Vpr in microtubule-dependent trafficking.

The initial formation of phagosomes is dependent on the actin cytoskeleton, but late intracellular trafficking of phagosomes to the cell center is mediated predominantly by microtubules (Desjardins et al., 1994; Blocker et al., 1996, 1998; Harrison et al., 2003). There are connections between the microtubule cytoskeleton and the machinery driving membrane fusion. The Rab7-interacting lysosomal protein, an effector of Rab7 and a marker of late endosomes/phagosomes, binds to the v-ATPase complex, p150Glued, and the Vps11 subunit of the homotypic fusion and protein sorting complex and is important for the biogenesis of phagolysosomes and bacterial clearance (Harrison et al., 2003, 2004; Johansson et al., 2007; van der Kant et al., 2013; De Luca et al., 2014). These machineries were recently shown to be modified in HIV-infected cells (Araínga et al., 2015). In our study, we report modified trafficking events implicating EHD3 and MICAL-L1, which participate in sorting events by controlling tubulation at the level of recycling or late endosomes (Abou-Zeid et al., 2011; Naslavsky and Caplan, 2011; Cai et al., 2013). We show for the first time that MICAL-L1 is required for efficient phagosomal maturation. Unexpectedly, EHD3 was enriched on the viral compartment. This sequestration could impair its function in endocytic/phagocytic trafficking and contribute to the defect in phagosomal maturation in HIV-1–infected macrophages.

Live cell imaging of HIV-infected macrophages revealed that the movement of phagosomes was slower after formation of the closed internalized compartment. Treating the cells with low doses of nocodazole or taxol, which are known now to displace the +TIPs such as EB1 (Akhmanova and Steinmetz, 2010; Gouveia and Akhmanova, 2010), slowed down the perinuclear accumulation of phagosomes approximately twofold (Blocker et al., 1998). Interestingly in neurons and filamentous fungi, it has been shown that microtubule plus end tracking of dynein is critical for correct initiation of retrograde cargo transport (Zhang et al., 2010; Moughamian and Holzbaur, 2012). More recently, an elegant in vitro reconstitution system determined that EB1 recruits $p150^{Glued}$ to target the dynein/dynactin complex to the plus ends of microtubules (Duellberg et al., 2014). In our study, ectopic expression of Vpr confirmed that this viral factor is sufficient to induce a defect in the initial EB1 loading of dynein motors on the plus ends of microtubules that is necessary for phagosome maturation. The differential location of phagosomes in infected macrophages will then affect the efficiency of fusion with other endosomal and lysosomal compartments, delaying the acquisition of hydrolytic activities.

Our data argue for a model (Fig. 8 E) in which the phagosomes formed in HIV-1–infected macrophages do not move efficiently onto the microtubules to reach the cell center because of impaired plus end loading of $p150^{Glued}$ by EB1, which is mislocalized by Vpr. They show altered sorting events and the hijacking of the EHD3 and MICAL-L1 components of the sorting machinery. Altogether, these results provide a mechanistic understanding of the defects in bacterial killing and clearance that contribute to the establishment of opportunistic infections in HIV-infected patients.

Materials and methods

Antibodies and reagents

The following primary antibodies were used: purified rabbit anti–SRBCs (IGN Biochemicals), rabbit anti–p65/RelA (sc-372; Santa Cruz Biotechnology), rabbit monoclonal anti–phospho-p65 (Ser536, 3033; Cell Signaling Technology), mAb anti-tubulin (clone DM1A; Sigma-Aldrich), mAb anti–phospho-p44/42 MAPK (Thr202/Tyr204) and anti-p44/42 MAPK (9106 and 9102, respectively; Cell Signaling Technology), rabbit monoclonal anti–phospho-SAPK/JNK (Thr183/Tyr185) and anti-SAPK/JNK (4668 and 9258, respectively; Cell Signaling Technology), rabbit monoclonal anti–phospho-p38 MAPK (Thr180/Tyr182) and rabbit anti–p38 (9215 and 9212, respectively, Cell Signaling Technology), mouse mAb anti–EHD3 (clone 4B7; Abnova Corporation), mouse monoclonal anti–LAMP1 (555798; BD Biosciences), mouse monoclonal anti–EEA1 (610456; BD Biosciences), mouse monoclonal anti–EB1 (610535; BD Biosciences; or sc-47704; Santa Cruz Biotechnology), mouse monoclonal anti–$p150^{Glued}$ (610473; BD Biosciences), mouse monoclonal anti–clathrin HC (610500; BD Biosciences), goat anti–p24 HIV-1 (4999-9007; AbD Serotec), mouse monoclonal anti–p24 HIV-1 (Kal-1; AbD Serotec), rabbit polyclonal anti–HA (H6908; Sigma-Aldrich), mouse monoclonal anti–HA (MMS-101P; BioLegend), rabbit polyclonal anti–DHC (sc-9115; Santa Cruz Biotechnology), and the recombinant human Fc anti–tubulin (clone F2C was obtained from the Antibody and Recombinant Proteins Facility, Institut Curie; Moutel et al., 2009). Rabbit polyclonal anti–MICAL-L1 was described in Abou-Zeid et al. (2011). In brief, the GST-MICAL-L1-RBD was generated by inserting a BamHI–XhoI fragment into the corresponding sites of a pGEX-4T expression vector and expressed in *Escherichia coli*. Purified GST-MICAL-L1-RBD was injected into rabbits to generate polyclonal antibodies (Covalab). The resulting antiserum was affinity purified against a His-RBD-Sepharose column.

Secondary antibodies were as follows: AMCA-, Cy2-, and Cy3-labeled $F(ab')_2$ anti–mouse IgG; Cy5-labeled $F(ab')_2$ anti–human IgG; AMCA- and Cy5-labeled $F(ab')_2$ anti–rabbit IgG; Cy5-labeled $F(ab')_2$ anti–rat IgG and Cy2-labeled $F(ab')_2$ anti–goat IgG; and HRP-labeled anti–mouse and anti–rabbit IgG (Jackson ImmunoResearch). Alexa Fluor 350/633–coupled phalloidins were obtained from Molecular Probes (Invitrogen).

siRNA sequences were as follows: 5′-GUCCCAGUAUUAC AACCACUU-3′ (MICAL-L1 1) and 5′-GUGGAGCCUAGAGUGGAA CAA-3′ (MICAL-L1 2; Abou-Zeid et al., 2011) to target MICAL-L1, and 5′-GCUGCGUGCCGGGGGCGAGCG-3′ to target EHD3 (Naslavsky et al., 2009). The control siRNA-targeting GFP was 5′-GAACGGCA UCAAGGUGAAC-3′.

The pcDNA3-HA plasmid was used as the control (from C. Lamaze, Institut Curie, Paris, France). The VprLai gene was subcloned into a pAS1B plasmid using the BamH1–XhoI sites. This vector contains an initiation codon, followed by the nucleotide sequence encoding the nine–amino acid epitope tag from the influenza virus HA and thus allows expression, driven by the cytomegalovirus promoter, of Vpr molecules fused at their N termini to HA (HA-tagged Vpr; Selig et al., 1999).

Carboxylated 3-µm silica H_2DCFDA-OxyBURST and DQ-BSA beads were as described (Podinovskaia et al., 2013). Nocodazole and lipopolysaccharide were from Sigma-Aldrich. Raltegravir was a

kind gift from Gianfranco Pancino (Institut Pasteur, Paris, France). polyinosinic:polycytidylic acid was purchased from Invivogen.

Cell culture and transfection

Human primary macrophages were isolated from blood of healthy donors (Etablissement Français du Sang Ile-de-France, Site Saint Vincent de Paul, Trinité, or Saint-Antoine) by density gradient sedimentation in Ficoll (GE Healthcare), followed by adhesion on plastic at 37°C for 2 h and culture in the presence of complete culture medium (RPMI 1640 supplemented with 10% FCS, 100 µg/ml streptomycin/penicillin, and 2 mM L-glutamine [Invitrogen/Gibco] containing 10 ng/ml recombinant macrophage-colony stimulating factor [R&D Systems]; Mazzolini et al., 2010). Treatment with siRNA was obtained after 72 h with Lipofectamine RNAiMAX reagent (Invitrogen; Marion et al., 2012). Transient nucleofection of 5-d differentiated monocytes (5×10^5 cells/cuvette) with expression plasmids was performed using Amaxa with Ingenio solution (Mirus Bio LLC; Jacquot et al., 2007; Mazzolini et al., 2010). HeLa cells were cultured in DMEM containing 25 mM D-glucose, GlutaMAX, and 1 mM sodium pyruvate (Life Technologies) supplemented with 10% FCS (Eurobio). They were transiently transfected using 10 µl Lipofectamine 2000 Transfection Reagent (Life Technologies) and 20 µg plasmid for a 100-mm subconfluent dish (Falcon).

Viral production and infection

Proviral infectious clones of the macrophage-tropic virus isolate ADA (HIV-1_{ADA}WT), and the same clone disrupted for the Nef ORF (HIV-$1_{ADA}\Delta$Nef) were kindly provided by Luciana da Costa (Federal University; Mazzolini et al., 2010). Proviral infectious clones of the macrophage-tropic virus isolate YU-2 (HIV-1_{Yu2}WT) were from the National Institutes of Health AIDS Research and Reference Reagent Program. The same clone disrupted for the Vpr gene HIV-$1_{Yu2}\Delta$Vpr was generated by PCR to insert two stop codons within the vpr gene without altering the vif gene, using the following set of primers: forward 5′-GATAGATG GAATAAGCCCCAGAAGACTAAGGGCCACAGAGG-3′, and reverse 5′-CCTCTGTGGCCCTTAGTCTTCTGGGGCTTATTCCATCTATC-3′ (Jacquot et al., 2007). The NLR 4.3 HIV-1Gag-iGFP carrying an R5-tropic envelope with the V3-loop V92th014.12 was a gift from M. Schindler (Helmholtz Zentrum Munich and Deutsches Forschungszentrum fur Gesundheit und Umwelt, Munich, Germany; Koppensteiner et al., 2012a). Stocks of viruses were obtained by transfection of human embryonic kidney 293 T cells (CRL-1573, 2×10^6; ATCC) with 6 µg of the corresponding proviral DNA, using FuGENE 6 Transfection Reagent as recommended by the manufacturer (Promega). VSV-G pseudotyped virus (HIV-$1_{ADA\text{-}VSV\text{-}G}$WT) was generated by transfection of human embryonic kidney 293 T cells with 1.5 µg VSV-G vector (pMD.G) along with 4.5 µg HIV-1 proviral DNA (HIV-1_{ADA}WT). Supernatants of the transfected cells were collected after 48 h, filtered, stored at −80°C, and quantified for the HIV-1 CAp24 antigen by ELISA (Innotests HIV Antigen mAb [Innogenetics] and Alliance HIV-1 ELISA kit [PerkinElmer]). Viral titers were assessed by infection of the indicator cells HeLa TZM-bl (bearing the β-galactosidase gene under the control of HIV-1 LTR; National Institutes of Health Reagent Program) with serial dilutions of the stocks, followed by a β-galactosidase coloration of the cells and counting of blue cells.

Monocytes differentiated into macrophages for 11 d were seeded in six-well plates at a density of 5×10^5 to 1×10^6 cells/well and cultivated in complete culture medium. For the microscopy experiments, the cells were detached after 10 d of differentiation and placed on coverslips at 2×10^5 cells/well. At 11 d of differentiation, HIV-1 viruses (MOI 0.03) were added. Viruses were washed after 1 or 2 d, for HIV-1 VSV-G pseudotyped or WT, respectively, and cells were kept for 8 d or the indicated times before functional assays.

Phagocytosis assay and phagosome measurements

Phagocytosis assays mediated by Fc or CR3 receptors were performed with adherent cells plated on glass coverslips (Braun et al., 2004). For microscopy, red blood cells (RBCs) were washed in PBS and incubated with anti-RBC antibodies for 30 min at RT, then washed and resuspended in serum-free medium. After internalization of the IgG-RBCs for the indicated times, cells were fixed in 4% PFA (Sigma-Aldrich)/4% sucrose for 45 min at 4°C and external RBCs were labeled for 10 min with labeled $F(ab')_2$ anti–mouse or anti–rabbit IgG in PBS/1% BSA. Cells were then permeabilized with 0.05% saponin before labeling of the intracellular RBCs with AMCA-labeled $F(ab')_2$ anti–rabbit IgG and/or other primary antibodies in PBS/0.05% saponin/1% BSA. Fixation was different to detect microtubule-associated proteins: cells were fixed for 10 min in ethanol at −20°C, then in 4% paraformaldehyde for 15 min at RT and permeabilized in 0.15% Triton X-100/PBS. Fixation to detect MICAL-L1 and EHD3 was at 4% paraformaldehyde, followed by permeabilization in 0.15% Triton X-100/PBS. Mounting medium was Fluoromont-G (eBioscience).

To quantify phagocytosis, the number of internalized RBCs per cell was counted in 10–50 cells randomly chosen on the coverslips (>200 phagosomes, identified by combination of phase-contrast and fluorescent images), corresponding to the phagocytic index. The index obtained was divided by the index obtained for control cells and was expressed as a percentage of control cells. To quantify the recruitment of LAMP1 on the internalized phagosomes, images were acquired and the presence of the marker on internalized phagosomes was analyzed on a yes/no basis (>200 phagosomes per condition). The number of LAMP1-positive phagosomes was divided by the number of total internal phagosomes per condition and expressed as percentage. A minimum of three independent experiments (i.e., on different donors) was performed.

Image acquisition was performed on an inverted wide-field microscope (DMI6000; Leica) with a 100× (1.4 NA) objective and a MicroMAX camera (Princeton Instruments) or ORCA Flash4.0 (Hamamatsu). Z-series of images were taken at 0.2-µm increments and deconvolution was performed with Huygens software (Scientific Volume Imaging) when indicated. Analyses were performed using custom-made ImageJ (National Institutes of Health) routines or Icy software. 3D reconstructions were obtained using the IsoSurface function in Imaris 5.7 software.

To quantify the number of comet-shaped structures in EB1-labeled macrophages, Z projection of maximum intensities of the images, TopHatFilter, and a fixed threshold were used to segment and calculate the circularity of all objects. Ellipsoid objects (circularity <0.5), corresponding to comets, were then counted. To quantify localization of EB1 and $p150^{Glued}$ within the cell volume, we used the Icy software ROI Statistics tool.

Depolymerization/repolymerization of microtubules

After 8 d of infection, macrophages were incubated in complete culture medium with or without nocodazole (10 µM) for 1 h at 37°C with 5% CO_2. After washing with cold complete culture medium, cells were placed at 37°C for various times before fixation with 100% ethanol at −20°C for 10 min and 4% PFA at room temperature for 15 min. Cells were then permeabilized with 0.15% Triton X-100 (Sigma-Aldrich) at 4°C for 2 min before labeling with antibodies and image analysis as described in the previous paragraph.

Phagosomal bead assay and flow cytometry analysis

H_2DCFDA-OxyBURST beads were coupled to H_2DCFDA and Alexa Fluor 633-SE (Molecular Probes). The oxidized substrate emitted a fluorescent signal at 520 nm when excited at 490 nm, and Alexa Fluor 633

emitted at 647 nm when excited at 633 nm. DQ-BSA beads were coupled to DQ green BSA and calibrated to Alexa Fluor 633-SE. The hydrolyzed substrate emitted at 520 nm when excited at 490 nm (Podinovskaia et al., 2013). Beads were extensively washed and incubated with HIV-1– or mock-infected macrophages in six-well plates in serum-free medium at 37°C. At each time point, cells were detached and washed twice before fixation with 4% PFA for 45 min at 4°C. PFA was neutralized with NH_4Cl (50 mM in PBS). Cells were washed with PBS and analyzed by flow cytometry (FACSCalibur or Accuri C6; BD Biosciences). The emission at 520 nm (substrate) and 650 nm (calibrator) was recorded after excitation at 488 and 635 nm, respectively. Analysis was performed using CellQuest Pro software (BD Biosciences). The number of cells containing substrate-positive beads was divided by the total number of cells containing beads and the results were expressed as a percentage.

Bacterial growth and plating assay

S. typhimurium (ATCC14028 or 4/74; Niedergang et al., 2000; Kröger et al., 2013, respectively) were grown overnight at 37°C with shaking in Luria-Bertani (LB) broth and then subcultured without shaking for 4–5 h in LB containing 300 mM NaCl (*S. typhimurium*). The absorbance at 600 nm of the bacterial suspensions was used to determine the MOI, by estimating that 10^9 bacteria/ml give an A_{600} of 1. The inoculum dose was then calculated by plating serial dilutions onto LB agar plates. MDMs were infected at a MOI of 50 in six-well plates. After a 30-min incubation at 37°C in 5% CO_2, the cells were washed two times with sterile PBS, washed once with complete RPMI medium supplemented with 50 µg/ml gentamicin, and then incubated in the latter medium for the indicated times. At each time point, cells were washed twice with PBS and lysed with 0.5% Triton X-100 in PBS. The number of viable bacteria present at each time point was determined by plating serial dilutions on LB agar plates.

Immunoprecipitation and Western blots

Cells were lysed for 15 min at 4°C in lysis buffer (20 mM Tris HCl, pH 7.5, 150 mM NaCl, 0.5% NP-40, 50 mM NaF, and 1 mM sodium orthovanadate, supplemented with complete protease inhibitor cocktail; Roche Diagnostic). Lysates were centrifuged at 10,000 *g* for 10 min at 4°C. The postnuclear supernatants were kept and an equal amount of proteins (BCA dosage kit; Pierce) was analyzed by SDS-PAGE. Immunoprecipitation was performed with HeLa cell lysates incubated with 4 µg rabbit anti–HA antibody for 1 h, followed by a 3-h incubation with Protein G beads. Proteins were transferred onto polyvinylidene difluoride membrane (Millipore) and incubated in blocking solution PBS/0.1% Tween-20 supplemented with 5% milk for 2 h. Blots were rinsed with PBS/0.1% Tween-20 and antibodies were incubated in the blocking solution. Detection was performed using ECL substrate (GE Healthcare). For mass spectrometry analysis, digestion was performed on beads and samples were desalted (ZipTip C18) and then analyzed with an nanoESI-Orbitrap on the LTQ-Orbitrap Fusion with nano-LC Proxeon 1000 (Thermo Fisher Scientific; Mass Spectrometry Facility, Institut Jacques Monod, Paris, France).

Cytokine arrays

Supernatants of primary macrophages were collected after 6 h of stimulation and were incubated with membranes containing primary antibody against different cytokines as indicated by the manufacturer (RayBio Human Cytokines Antibody Array kit; Cliniscience). The ECL signal was quantified and the semiquantitative results were summarized in a table in Fig. 1 H.

Live cell imaging of phagocytosis in HIV-1–infected primary macrophages

To follow phagocytosis on HIV-1 GFP–infected or noninfected cells, images were recorded every min for 2 h on a spinning disk confocal (CSU-X1M1; Yokogawa) inverted microscope (DMI6000; Leica) equipped with a CoolSnap HQ^2 camera (Photometrics) and a heated chamber and CO_2 in the BSL3 laboratory. HIV-1–GFP and SRBCs were visualized by fluorescence and phase contrast with a 100×, 1.4 NA, PH differential interference contrast objective. Acquisition was performed with MetaMorph 7.5.5 software (Molecular Devices). The movies were analyzed using ImageJ with the Manual Tracking Plugin (F. Cordelières, Institut Curie, Orsay, France). Distances relative to the nucleus (visible on phase contrast images) were calculated in micrometers and the traveled distances were calculated and plotted against time. The slopes were calculated with linear regression.

Proximity ligation in situ assay (Duolink)

The Duolink proximity ligation in situ assay (Söderberg et al., 2006) was used according to the manufacturer's instructions. Anti–HA rabbit polyclonal Ab was combined with anti–EB1 mouse mAb or anti–$p150^{Glued}$ mouse mAb and anti–HA mouse monoclonal Ab was combined with anti–DHC rabbit mAb. The positive control was obtained using a combination of anti–α-tubulin mouse mAb and anti–DHC rabbit mAb. Negative controls were performed by omitting anti–HA rabbit antibodies. Fluorescent spots generated were automatically counted and the mean number of spots per cell was calculated from nuclei counting using the Icy software SpotDetector function.

Statistical analyses

The statistical significance of the data was tested with an unpaired Student's *t* test. Differences were considered significant if the p-value was <0.05 and 0.005.

Online supplemental material

Fig. S1 (related to Fig. 2) shows detection of hydrolytic and oxidative activity in macrophages infected or not with HIV-1. Fig. S2 (related to Fig. 3) shows the depletion of MICAL-L1 and EHD3 in human MDMs upon treatment with siRNA. Video 1 shows the internalization of IgG-opsonized RBCs in noninfected human MDMs. Video 2 shows the internalization of IgG-opsonized RBCs in HIV-infected human MDMs. Online supplemental material is available at http://www.jcb.org/cgi/content/full/jcb.201503124/DC1. Additional data are available in the JCB DataViewer at http://dx.doi.org/10.1083/jcb.201503124.dv.

Acknowledgments

We thank Marie N'Guyen for help with the Imagestream technology, the Mass Spectrometry Facility at Institut Jacques Monod, Clarisse Berlioz-Torrent for help with viral production, Chantal Deschamps and Melita Gordon for discussions, and Jamil Jubrail for reading the manuscript.

This work was supported by grants from the Centre National de la Recherche Scientifique, Institut National de la Santé et de la Recherche Médicale, Université Paris Descartes, Agence Nationale de Recherches sur le Sida et les Hépatites (ANRS; AO2010-1 and AO2012-2 to S. Benichou and F. Niedergang), Agence Nationale de la Recherche (2011 BSV3 025 02), and Fondation pour la Recherche Médicale (DEQ20130326518 to F. Niedergang). D.G. Russell acknowledges support from the National Institutes of Health (award HL100928). J. Mazzolini was supported by a doctoral fellowship from ANRS. A. Dumas was supported by doctoral fellowships from Université Paris Descartes and Sidaction.

The authors declare no competing financial interests.

Submitted: 26 March 2015
Accepted: 18 September 2015

References

Abou-Zeid, N., R. Pandjaitan, L. Sengmanivong, V. David, G. Le Pavec, J. Salamero, and A. Zahraoui. 2011. MICAL-like1 mediates epidermal growth factor receptor endocytosis. *Mol. Biol. Cell.* 22:3431–3441. http://dx.doi.org/10.1091/mbc.E11-01-0030

Akhmanova, A., and M.O. Steinmetz. 2010. Microtubule +TIPs at a glance. *J. Cell Sci.* 123:3415–3419. http://dx.doi.org/10.1242/jcs.062414

Araínga, M., D. Guo, J. Wiederin, P. Ciborowski, J. McMillan, and H.E. Gendelman. 2015. Opposing regulation of endolysosomal pathways by long-acting nanoformulated antiretroviral therapy and HIV-1 in human macrophages. *Retrovirology.* 12:5. http://dx.doi.org/10.1186/s12977-014-0133-5

Blocker, A., F.F. Severin, A. Habermann, A.A. Hyman, G. Griffiths, and J.K. Burkhardt. 1996. Microtubule-associated protein-dependent binding of phagosomes to microtubules. *J. Biol. Chem.* 271:3803–3811. http://dx.doi.org/10.1074/jbc.271.7.3803

Blocker, A., G. Griffiths, J.C. Olivo, A.A. Hyman, and F.F. Severin. 1998. A role for microtubule dynamics in phagosome movement. *J. Cell Sci.* 111:303–312.

Botelho, R.J., and S. Grinstein. 2011. Phagocytosis. *Curr. Biol.* 21:R533–R538. http://dx.doi.org/10.1016/j.cub.2011.05.053

Braun, V., V. Fraisier, G. Raposo, I. Hurbain, J.B. Sibarita, P. Chavrier, T. Galli, and F. Niedergang. 2004. TI-VAMP/VAMP7 is required for optimal phagocytosis of opsonised particles in macrophages. *EMBO J.* 23:4166–4176. http://dx.doi.org/10.1038/sj.emboj.7600427

Cai, B., S.S. Giridharan, J. Zhang, S. Saxena, K. Bahl, J.A. Schmidt, P.L. Sorgen, W. Guo, N. Naslavsky, and S. Caplan. 2013. Differential roles of C-terminal Eps15 homology domain proteins as vesiculators and tubulators of recycling endosomes. *J. Biol. Chem.* 288:30172–30180. http://dx.doi.org/10.1074/jbc.M113.488627

Canton, J., D. Neculai, and S. Grinstein. 2013. Scavenger receptors in homeostasis and immunity. *Nat. Rev. Immunol.* 13:621–634. http://dx.doi.org/10.1038/nri3515

Carter, C.A., and L.S. Ehrlich. 2008. Cell biology of HIV-1 infection of macrophages. *Annu. Rev. Microbiol.* 62:425–443. http://dx.doi.org/10.1146/annurev.micro.62.081307.162758

Collman, R.G., C.F. Perno, S.M. Crowe, M. Stevenson, and L.J. Montaner. 2003. HIV and cells of macrophage/dendritic lineage and other non-T cell reservoirs: new answers yield new questions. *J. Leukoc. Biol.* 74:631–634. http://dx.doi.org/10.1189/jlb.0703357

De Luca, M., L. Cogli, C. Progida, V. Nisi, R. Pascolutti, S. Sigismund, P.P. Di Fiore, and C. Bucci. 2014. RILP regulates vacuolar ATPase through interaction with the V1G1 subunit. *J. Cell Sci.* 127:2697–2708. http://dx.doi.org/10.1242/jcs.142604

Deschamps, C., A. Echard, and F. Niedergang. 2013. Phagocytosis and cytokinesis: do cells use common tools to cut and to eat? Highlights on common themes and differences. *Traffic.* 14:355–364. http://dx.doi.org/10.1111/tra.12045

Desjardins, M., L.A. Huber, R.G. Parton, and G. Griffiths. 1994. Biogenesis of phagolysosomes proceeds through a sequential series of interactions with the endocytic apparatus. *J. Cell Biol.* 124:677–688. http://dx.doi.org/10.1083/jcb.124.5.677

Duellberg, C., M. Trokter, R. Jha, I. Sen, M.O. Steinmetz, and T. Surrey. 2014. Reconstitution of a hierarchical +TIP interaction network controlling microtubule end tracking of dynein. *Nat. Cell Biol.* 16:804–811. http://dx.doi.org/10.1038/ncb2999

Fackler, O.T., and A.S. Baur. 2002. Live and let die: Nef functions beyond HIV replication. *Immunity.* 16:493–497. http://dx.doi.org/10.1016/S1074-7613(02)00307-2

Fairn, G.D., and S. Grinstein. 2012. How nascent phagosomes mature to become phagolysosomes. *Trends Immunol.* 33:397–405. http://dx.doi.org/10.1016/j.it.2012.03.003

Flannagan, R.S., V. Jaumouillé, and S. Grinstein. 2012. The cell biology of phagocytosis. *Annu. Rev. Pathol.* 7:61–98. http://dx.doi.org/10.1146/annurev-pathol-011811-132445

Foster, J.L., and J.V. Garcia. 2008. HIV-1 Nef: at the crossroads. *Retrovirology.* 5:84. http://dx.doi.org/10.1186/1742-4690-5-84

Gaudin, R., S. Berre, B. Cunha de Alencar, J. Decalf, M. Schindler, F.X. Gobert, M. Jouve, and P. Benaroch. 2013. Dynamics of HIV-containing compartments in macrophages reveal sequestration of virions and transient surface connections. *PLoS ONE.* 8:e69450. http://dx.doi.org/10.1371/journal.pone.0069450

Gouveia, S.M., and A. Akhmanova. 2010. Cell and molecular biology of microtubule plus end tracking proteins: end binding proteins and their partners. *Int. Rev. Cell Mol. Biol.* 285:1–74. http://dx.doi.org/10.1016/B978-0-12-381047-2.00001-3

Guenzel, C.A., C. Hérate, and S. Benichou. 2014. HIV-1 Vpr-a still "enigmatic multitasker". *Front. Microbiol.* 5:127. http://dx.doi.org/10.3389/fmicb.2014.00127

Harrison, R.E., C. Bucci, O.V. Vieira, T.A. Schroer, and S. Grinstein. 2003. Phagosomes fuse with late endosomes and/or lysosomes by extension of membrane protrusions along microtubules: role of Rab7 and RILP. *Mol. Cell. Biol.* 23:6494–6506. http://dx.doi.org/10.1128/MCB.23.18.6494-6506.2003

Harrison, R.E., J.H. Brumell, A. Khandani, C. Bucci, C.C. Scott, X. Jiang, B.B. Finlay, and S. Grinstein. 2004. *Salmonella* impairs RILP recruitment to Rab7 during maturation of invasion vacuoles. *Mol. Biol. Cell.* 15:3146–3154. http://dx.doi.org/10.1091/mbc.E04-02-0092

Jacquot, G., E. Le Rouzic, A. David, J. Mazzolini, J. Bouchet, S. Bouaziz, F. Niedergang, G. Pancino, and S. Benichou. 2007. Localization of HIV-1 Vpr to the nuclear envelope: impact on Vpr functions and virus replication in macrophages. *Retrovirology.* 4:84. http://dx.doi.org/10.1186/1742-4690-4-84

Jambo, K.C., D.H. Banda, A.M. Kankwatira, N. Sukumar, T.J. Allain, R.S. Heyderman, D.G. Russell, and H.C. Mwandumba. 2014. Small alveolar macrophages are infected preferentially by HIV and exhibit impaired phagocytic function. *Mucosal Immunol.* 7:1116–1126. http://dx.doi.org/10.1038/mi.2013.127

Johansson, M., N. Rocha, W. Zwart, I. Jordens, L. Janssen, C. Kuijl, V.M. Olkkonen, and J. Neefjes. 2007. Activation of endosomal dynein motors by stepwise assembly of Rab7-RILP-p150Glued, ORP1L, and the receptor betalll spectrin. *J. Cell Biol.* 176:459–471. http://dx.doi.org/10.1083/jcb.200606077

Jouve, M., N. Sol-Foulon, S. Watson, O. Schwartz, and P. Benaroch. 2007. HIV-1 buds and accumulates in "nonacidic" endosomes of macrophages. *Cell Host Microbe.* 2:85–95. http://dx.doi.org/10.1016/j.chom.2007.06.011

Kedzierska, K., and S.M. Crowe. 2002. The role of monocytes and macrophages in the pathogenesis of HIV-1 infection. *Curr. Med. Chem.* 9:1893–1903. http://dx.doi.org/10.2174/0929867023368935

Kogan, M., and J. Rappaport. 2011. HIV-1 accessory protein Vpr: relevance in the pathogenesis of HIV and potential for therapeutic intervention. *Retrovirology.* 8:25. http://dx.doi.org/10.1186/1742-4690-8-25

Koppensteiner, H., C. Banning, C. Schneider, H. Hohenberg, and M. Schindler. 2012a. Macrophage internal HIV-1 is protected from neutralizing antibodies. *J. Virol.* 86:2826–2836. http://dx.doi.org/10.1128/JVI.05915-11

Koppensteiner, H., R. Brack-Werner, and M. Schindler. 2012b. Macrophages and their relevance in Human Immunodeficiency Virus Type I infection. *Retrovirology.* 9:82. http://dx.doi.org/10.1186/1742-4690-9-82

Kröger, C., A. Colgan, S. Srikumar, K. Händler, S.K. Sivasankaran, D.L. Hammarlöf, R. Canals, J.E. Grissom, T. Conway, K. Hokamp, and J.C. Hinton. 2013. An infection-relevant transcriptomic compendium for *Salmonella enterica* Serovar Typhimurium. *Cell Host Microbe.* 14:683–695. http://dx.doi.org/10.1016/j.chom.2013.11.010

Marion, S., J. Mazzolini, F. Herit, P. Bourdoncle, N. Kambou-Pene, S. Hailfinger, M. Sachse, J. Ruland, A. Benmerah, A. Echard, et al. 2012. The NF-κB signaling protein Bcl10 regulates actin dynamics by controlling AP1 and OCRL-bearing vesicles. *Dev. Cell.* 23:954–967. http://dx.doi.org/10.1016/j.devcel.2012.09.021

Mazzolini, J., F. Herit, J. Bouchet, A. Benmerah, S. Benichou, and F. Niedergang. 2010. Inhibition of phagocytosis in HIV-1-infected macrophages relies on Nef-dependent alteration of focal delivery of recycling compartments. *Blood.* 115:4226–4236. http://dx.doi.org/10.1182/blood-2009-12-259473

McDonald, D., M.A. Vodicka, G. Lucero, T.M. Svitkina, G.G. Borisy, M. Emerman, and T.J. Hope. 2002. Visualization of the intracellular behavior of HIV in living cells. *J. Cell Biol.* 159:441–452. http://dx.doi.org/10.1083/jcb.200203150

Moretti, J., and J.M. Blander. 2014. Insights into phagocytosis-coupled activation of pattern recognition receptors and inflammasomes. *Curr. Opin. Immunol.* 26:100–110. http://dx.doi.org/10.1016/j.coi.2013.11.003

Moughamian, A.J., and E.L. Holzbaur. 2012. Dynactin is required for transport initiation from the distal axon. *Neuron.* 74:331–343. http://dx.doi.org/10.1016/j.neuron.2012.02.025

Moutel, S., A. El Marjou, O. Vielemeyer, C. Nizak, P. Benaroch, S. Dübel, and F. Perez. 2009. A multi-Fc-species system for recombinant antibody production. *BMC Biotechnol.* 9:14. http://dx.doi.org/10.1186/1472-6750-9-14

Naslavsky, N., and S. Caplan. 2011. EHD proteins: key conductors of endocytic transport. *Trends Cell Biol.* 21:122–131. http://dx.doi.org/10.1016/j.tcb.2010.10.003

Naslavsky, N., J. McKenzie, N. Altan-Bonnet, D. Sheff, and S. Caplan. 2009. EHD3 regulates early-endosome-to-Golgi transport and preserves Golgi morphology. *J. Cell Sci.* 122:389–400. http://dx.doi.org/10.1242/jcs.037051

Niedergang, F. 2016. Phagocytosis. In Encyclopedia of Cell Biology. Vol. 2. R.A. Bradshaw, and P.D. Stahl, editors. Elsevier, Waltham, MA. 751–757.

Niedergang, F., J.-C. Sirard, C.T. Blanc, and J.-P. Kraehenbuhl. 2000. Entry and survival of *Salmonella typhimurium* in dendritic cells and presentation of recombinant antigens do not require macrophage-specific virulence factors. *Proc. Natl. Acad. Sci. USA*. 97:14650–14655. http://dx.doi.org/10.1073/pnas.97.26.14650

Patel, P.C., K.H. Fisher, E.C. Yang, C.M. Deane, and R.E. Harrison. 2009. Proteomic analysis of microtubule-associated proteins during macrophage activation. *Mol. Cell. Proteomics.* 8:2500–2514. http://dx.doi.org/10.1074/mcp.M900190-MCP200

Planelles, V., and S. Benichou. 2009. Vpr and its interactions with cellular proteins. *Curr. Top. Microbiol. Immunol.* 339:177–200. http://dx.doi.org/10.1007/978-3-642-02175-6_9

Podinovskaia, M., W. Lee, S. Caldwell, and D.G. Russell. 2013. Infection of macrophages with *Mycobacterium tuberculosis* induces global modifications to phagosomal function. *Cell. Microbiol.* 15:843–859. http://dx.doi.org/10.1111/cmi.12092

Russell, D.G., and R.M. Yates. 2007. TLR signalling and phagosome maturation: an alternative viewpoint. *Cell. Microbiol.* 9:849–850. http://dx.doi.org/10.1111/j.1462-5822.2007.00920.x

Sabo, Y., D. Walsh, D.S. Barry, S. Tinaztepe, K. de Los Santos, S.P. Goff, G.G. Gundersen, and M.H. Naghavi. 2013. HIV-1 induces the formation of stable microtubules to enhance early infection. *Cell Host Microbe.* 14:535–546. http://dx.doi.org/10.1016/j.chom.2013.10.012

Scott, C.C., F. Vacca, and J. Gruenberg. 2014. Endosome maturation, transport and functions. *Semin. Cell Dev. Biol.* 31:2–10. http://dx.doi.org/10.1016/j.semcdb.2014.03.034

Selig, L., J.C. Pages, V. Tanchou, S. Prévéral, C. Berlioz-Torrent, L.X. Liu, L. Erdtmann, J. Darlix, R. Benarous, and S. Benichou. 1999. Interaction with the p6 domain of the gag precursor mediates incorporation into virions of Vpr and Vpx proteins from primate lentiviruses. *J. Virol.* 73:592–600.

Söderberg, O., M. Gullberg, M. Jarvius, K. Ridderstråle, K.J. Leuchowius, J. Jarvius, K. Wester, P. Hydbring, F. Bahram, L.G. Larsson, and U. Landegren. 2006. Direct observation of individual endogenous protein complexes in situ by proximity ligation. *Nat. Methods.* 3:995–1000. http://dx.doi.org/10.1038/nmeth947

Strebel, K. 2013. HIV accessory proteins versus host restriction factors. *Curr. Opin. Virol.* 3:692–699. http://dx.doi.org/10.1016/j.coviro.2013.08.004

van der Kant, R., A. Fish, L. Janssen, H. Janssen, S. Krom, N. Ho, T. Brummelkamp, J. Carette, N. Rocha, and J. Neefjes. 2013. Late endosomal transport and tethering are coupled processes controlled by RILP and the cholesterol sensor ORP1L. *J. Cell Sci.* 126:3462–3474. http://dx.doi.org/10.1242/jcs.129270

Witkowski, W., and B. Verhasselt. 2013. Contributions of HIV-1 Nef to immune dysregulation in HIV-infected patients: a therapeutic target? *Expert Opin. Ther. Targets.* 17:1345–1356. http://dx.doi.org/10.1517/14728222.2013.830712

Yates, R.M., and D.G. Russell. 2008. Real-time spectrofluorometric assays for the lumenal environment of the maturing phagosome. *Methods Mol. Biol.* 445:311–325. http://dx.doi.org/10.1007/978-1-59745-157-4_20

Yates, R.M., A. Hermetter, G.A. Taylor, and D.G. Russell. 2007. Macrophage activation downregulates the degradative capacity of the phagosome. *Traffic.* 8:241–250. http://dx.doi.org/10.1111/j.1600-0854.2006.00528.x

Zhang, J., L. Zhuang, Y. Lee, J.F. Abenza, M.A. Peñalva, and X. Xiang. 2010. The microtubule plus-end localization of *Aspergillus* dynein is important for dynein-early-endosome interaction but not for dynein ATPase activation. *J. Cell Sci.* 123:3596–3604. http://dx.doi.org/10.1242/jcs.075259